Monte Carlo simulation of the ferromagnetic order-disorder transition in a Heisenberg fluid

M. J. P. Nijmeijer and J. J. Weis
Laboratoire de Physique Théorique et Hautes Energies, Bâtiment 211, Université Paris-Sud, 91405 Orsay Cedex, France
(Received 15 June 1995)

We have simulated a fluid of particles which carry a Heisenberg spin and interact via a Heisenberg-like interaction. The fluid displays a magnetic order-disorder transition, which we studied by varying the temperature at a fixed particle density. We located the transition and estimated critical exponents by means of a finite-size scaling analysis. The exponents differ by a small but significant amount from the ones for the lattice Heisenberg model.

PACS number(s): 61.20.Ja, 64.60.Fr, 75.50.Ww

I. INTRODUCTION

Heisenberg fluids have recently been studied in Monte Carlo (MC) simulations by Lomba *et al.* [1] as simplified models of ferrofluids. The simulations established the occurrence of a liquid-vapor transition as well as a magnetic order-disorder transition in a ferromagnetic Heisenberg fluid [1]. Simulations of an antiferromagnetic Heisenberg fluid have been carried out as well [2]. They found no evidence for a liquid-vapor transition; however, a transition from a disordered phase to a phase with antiferromagnetic ordering (at least at a local scale) was observed. Throughout this paper we will restrict ourselves to the ferromagnetic case [1].

The simulations of Lomba *et al.* aimed at mapping out the phase diagram of the ferromagnetic Heisenberg fluid and focused on the interplay between the magnetic and the liquid-vapor transitions. They report evidence that a line of continuous magnetic order-disorder transitions ends at a first-order liquid-vapor line in a critical end point. The phase diagram has also been studied by means of the mean spherical approximation [3], mean field theory [4], and density-functional methods [5].

Since no finite-size effects have been accounted for in the simulations of Lomba *et al.*, the location of the transition temperature of the magnetic order-disorder transition is rather crude. The magnetization of a 500 particle system was recorded as a function of temperature (at fixed density) and the transition temperature was taken to be the temperature at which the magnetization was approximately 0.5. Similarly, the liquid-vapor coexistence densities were determined by Gibbs ensemble Monte Carlo (GEMC) calculations for a 500 particle system and no finite-size analysis was carried out. Bearing also in mind that the critical point cannot be approached closely with the GEMC method, it is likely that the simulation results in [1] are of insufficient quality to determine how the magnetic order-disorder line joins the liquid-vapor line.

Apart from the interplay between the magnetic order-disorder transition and the liquid-vapor transition, one can study the magnetic transition itself. In particular, one can question whether the magnetic transition in the Heisenberg fluid is in the same universality class as the transition in the lattice Heisenberg model. The Heisenberg fluid resembles a Heisenberg lattice model with an annealed site dilution [6]. A fixed particle density in the fluid corresponds to a fixed degree of dilution in the lattice. To the best of our knowledge, little is known about lattice models with a fixed density of annealed diluted sites. Quenched site dilution is predicted not to change the universality class of the lattice Heisenberg model [7,8]. Annealed bond dilution is thought to change critical exponents according to Fisher renormalization [6,9]. The Blume-Capel model is an example of a model (the Ising model) with an annealed site dilution. The density of annealed sites is, however, not fixed but can fluctuate around an average that is controlled by an external field [10,11].

A comparison of our results with those for the undiluted lattice Heisenberg model is facilitated by three recent MC studies of the undiluted lattice model [12–14]. They give accurate results for critical exponents and other critical parameters and are in excellent agreement with each other.

In this work we aim to carry out accurate simulations of the magnetic order-disorder transition in a Heisenberg fluid. We do not study the first-order liquid-vapor line or the way in which the two transitions are joined. Following Lomba *et al.* we vary the temperature at a fixed density. However, unlike Lomba *et al.* we truncate the particle potential at a fixed distance in all simulations and we use different system sizes to carry out a finite-size scaling (FSS) analysis. As a result, the accuracy is much improved and even permits us to estimate critical exponents.

The paper is organized as follows. Section II describes the model and technical aspects of the simulations. Results are given in Secs. III and IV. Conclusions are given in Sec. V. A short version of this paper has been presented elsewhere [15].

 ©1996 The American Physical Society

II. SIMULATIONS

We perform simulations of the three-dimensional Heisenberg fluid in the canonical ensemble. The particles are enclosed in a cubic box with periodic boundary conditions. The particles interact with the potential

$$\phi(\vec{r}_i,\vec{r}_j,\vec{s}_i,\vec{s}_j)=\begin{cases}\infty, & r_{ij}<\sigma\\ -J(r_{ij})\vec{s}_i\cdot\vec{s}_j, & \sigma<r_{ij}<2.5\sigma\\ 0, & r_{ij}>2.5\sigma\end{cases} \quad (1)$$

where $\phi(\vec{r}_i,\vec{r}_j,\vec{s}_i,\vec{s}_j)$ denotes the potential between a particle i with position $\vec{r}_i$ and spin $\vec{s}_i$ and a particle j with position $\vec{r}_j$ and spin $\vec{s}_j$. The spins are Heisenberg spins, i.e., each spin $\vec{s}_i$ is a three-dimensional vector of unit length. The hard-core repulsion at distances r_{ij} ($r_{ij}=|\vec{r}_i-\vec{r}_j|$) smaller than σ prohibits these interparticle distances while two particles further than 2.5σ away from each other do not interact. The Heisenberg-like interaction at distances r_{ij} in between has a ferromagnetic, Yukawa-type coupling constant:

$$J(r)=\epsilon\frac{\sigma}{r}\exp\left\{\frac{r-\sigma}{\sigma}\right\} \quad (2)$$

where ϵ sets the energy scale of the interaction. This potential is the same as that used in Ref. [1] except that we cut it at a distance 2.5σ.

We vary the temperature T in our simulations while keeping the density fixed. We do this for three densities n: $n=0.4$, $n=0.6$, and $n=0.7$ (all densities are expressed in units of σ^{-3}). The systems have a number of particles N ranging from $N=108$ to $N=1372$ (for $n=0.4$ and $n=0.7$) or from $N=108$ to $N=2916$ (for $n=0.6$). All systems are listed in Tables I–III.

The simulations need to sample spin degrees and positional degrees of freedom. The positions were sampled with a regular Metropolis scheme and the spin degrees of freedom with the Wolff algorithm [16]. The application of the Wolff algorithm to an off-lattice system is, as far as we know, a novelty but constitutes a straightforward generalization of the lattice version. Two modifications must be made: (a) one should take as neighbor particles of a particle i all particles within a distance of 2.5σ of the particle i; (b) one should recall that the coupling constant J (2) is not a constant as in a lattice with nearest-neighbor interactions but depends on the distance r_{ij} between the neighboring particles i and j. With these two modifications, the algorithm of Ref. [16] applies also to our off-lattice system. Detailed balance and ergodicity of the algorithm hold for the off-lattice version for the same reasons as for the lattice version.

The sequence of system updates in the MC calculations is as follows: two sweeps, in each of which we attempt to move each particle once, are followed by the construction of one Wolff cluster after which the Monte Carlo proceeds with the next two sweeps. We chose the maximum position displacement such that the acceptance ratio of the trial moves was around 50%. The size of the Wolff cluster around T_c varied between 13–15 % of the total number of particles N for $N=108$ to 5–6 % for $N=1372$ and $N=2916$. A system is typically followed for 10^6 sweeps with the corresponding 0.5×10^6 Wolff updates. Precise run lengths are given in Tables I–III.

After each sweep we measure the energy U of the system; after each Wolff update we measure the magnetization $\vec{m}$, defined as

$$\vec{m}=\frac{1}{N}\sum_{i=1}^{N}\vec{s}_i. \quad (3)$$

In each simulation (carried out at a fixed N, n, and T) we calculate the average magnetization moments $\langle m^k\rangle_{mc}$ $m=|\vec{m}|$, $k=1,2,3,4$, and the subscript mc stands for

TABLE I. Simulated systems at the density $n=0.4$. N is the number of particles in the system; T is the temperature of the system; N_s is the number of sweeps (in millions) in the simulation (the number of Wolff updates is half the number of sweeps); $\langle u\rangle$ is the energy per particle averaged over the simulation; the $\langle m^k\rangle$ are the average magnetization moments ($k=1,2,3,4$). The values between parentheses are the errors on the last decimal.

N	T	N_S 10^6	$\langle u\rangle$	$\langle m\rangle$	$\langle m^2\rangle$	$\langle m^3\rangle$	$\langle m^4\rangle$
108	1.9	1.2	-0.980(2)	0.4538(6)	0.2142(5)	0.1043(3)	0.0520(2)
108	1.95	1.2	-0.894(2)	0.4241(6)	0.1890(5)	0.0874(3)	0.0417(2)
108	2	1.2	-0.813(2)	0.3937(7)	0.1648(5)	0.0722(3)	0.0382(2)
108	2.05	1.2	-0.739(2)	0.3651(7)	0.1436(5)	0.0596(3)	0.0258(1)
256	1.9	1.08	-0.923(1)	0.3967(6)	0.1631(4)	0.0690(3)	0.0299(1)
256	1.95	1.08	-0.832(1)	0.3580(6)	0.1348(4)	0.0528(2)	0.0213(1)
256	2	1.26	-0.748(1)	0.3206(6)	0.1100(4)	0.0397(2)	0.01490(9)
256	2.05	1.08	-0.676(1)	0.2866(7)	0.0895(4)	0.0297(2)	0.01036(8)
500	1.9	0.984	-0.899(1)	0.3607(6)	0.1344(4)	0.0514(2)	0.0201(1)
500	1.95	0.96	-0.803(1)	0.3138(7)	0.1037(4)	0.0356(2)	0.01265(8)
500	2	0.96	-0.717(1)	0.2691(7)	0.0780(4)	0.0239(2)	0.00763(7)
500	2.05	0.98	-0.645(1)	0.2299(7)	0.0583(3)	0.0159(1)	0.00457(4)
1372	1.93	0.9	-0.8149(9)	0.2798(6)	0.0816(3)	0.0246(1)	0.00760(6)
1372	1.96	0.9	-0.7556(9)	0.2432(7)	0.0629(3)	0.0170(1)	0.00477(4)
1372	1.99	0.9	-0.703(1)	0.2089(7)	0.0475(3)	0.01146(9)	0.00290(3)

TABLE II. As Table I for the density $n = 0.6$.

N	T	N_S 10^6	$\langle u \rangle$	$\langle m \rangle$	$\langle m^2 \rangle$	$\langle m^3 \rangle$	$\langle m^4 \rangle$
108	3.1	1.2	-1.247(3)	0.4341(6)	0.1971(5)	0.0926(3)	0.0448(2)
108	3.15	1.2	-1.163(3)	0.4147(7)	0.1811(5)	0.0822(3)	0.0385(2)
108	3.2	1.2	-1.089(3)	0.3965(6)	0.1668(5)	0.0733(3)	0.0333(2)
256	3.05	1	-1.229(2)	0.4037(6)	0.1684(4)	0.0721(3)	0.0316(1)
256	3.1	1.1	-1.130(2)	0.3778(6)	0.1488(4)	0.0605(2)	0.0253(1)
256	3.15	1.08	-1.042(2)	0.3532(6)	0.1314(4)	0.0508(2)	0.0202(1)
256	3.2	1.08	-0.954(2)	0.3270(7)	0.1139(4)	0.0416(2)	0.0157(1)
256	3.25	1	-0.879(2)	0.3043(7)	0.0997(4)	0.0345(2)	0.01243(9)
500	3.05	1	-1.179(2)	0.3724(6)	0.1425(4)	0.0558(2)	0.0223(1)
500	3.1	1.08	-1.072(2)	0.3412(6)	0.1210(4)	0.0442(2)	0.01654(9)
500	3.15	1.12	-0.979(2)	0.3112(7)	0.1020(4)	0.0348(2)	0.01224(8)
500	3.2	1.08	-0.889(2)	0.2801(7)	0.0840(4)	0.0265(2)	0.00868(7)
500	3.25	1	-0.813(2)	0.2531(7)	0.0697(3)	0.0204(1)	0.00623(5)
1372	3.13	1.12	-0.959(1)	0.2731(6)	0.0778(3)	0.0229(1)	0.00691(5)
1372	3.16	1.12	-0.898(2)	0.2487(6)	0.0654(3)	0.0179(1)	0.00508(4)
1372	3.19	1	-0.839(2)	0.2235(7)	0.0537(3)	0.0136(1)	0.00358(3)
2916	3.12	0.52	-0.952(2)	0.2515(8)	0.0655(4)	0.0175(1)	0.00480(5)
2916	3.15	0.48	-0.886(2)	0.220(1)	0.0512(4)	0.0124(1)	0.00309(4)
2916	3.18	0.48	-0.829(2)	0.1926(9)	0.0398(3)	0.0087(1)	0.00197(3)

microcanonical) as a function of the energy per particle u of the system and we sample the energy distribution $P(u;T,N,n)$. With the multihistogram technique we can then, for given N and n, construct the energy distribution for all temperatures T around the temperatures $\{T_i\}$ at which we performed the simulations [17]. The energy distribution permits us to calculate, e.g., the canonical averages $\langle m^k \rangle$ of the magnetization moments:

$$\langle m^k \rangle(T,N,n) = \int du\ \langle m^k \rangle_{mc}(u;N,n)\ P(u;T,N,n) \tag{4}$$

[13]. Canonical averages $\langle u^k \rangle$ of moments of the energy and cross-correlations between energy and magnetization such as $\langle um \rangle$ can be calculated in the same way.

Both the microcanonical averages and the energy distribution are calculated on a grid of 4096 bins in the energy interval between $u = -5$ and $u = 0$ (all energies are given in units of ϵ). To check the effects of this discretization we averaged during each simulation 100 consecutive measurements of the energy and 50 consecutive measurements of the magnetization moments and stored those subaverages. The averages of the subaverages are the canonical averages $\langle u \rangle$ and $\langle m^k \rangle$ $(k = 1,2,3,4)$ for the N, n, and T at which we performed the simulation. They are direct averages over the configurations that occurred in the simulation run and are not affected by an

TABLE III. As Table I for the density $n = 0.7$.

N	T	N_S 10^6	$\langle u \rangle$	$\langle m \rangle$	$\langle m^2 \rangle$	$\langle m^3 \rangle$	$\langle m^4 \rangle$
108	3.75	1.2	-1.361(3)	0.4220(6)	0.1870(5)	0.0860(3)	0.0407(2)
108	3.8	1.2	-1.280(3)	0.4055(6)	0.1739(5)	0.0777(3)	0.0358(2)
108	3.85	1.2	-1.198(3)	0.3886(6)	0.1608(5)	0.0697(3)	0.0313(2)
108	3.9	1.2	-1.129(3)	0.3739(6)	0.1498(5)	0.0631(3)	0.0276(1)
256	3.75	1.6	-1.216(2)	0.3654(5)	0.1398(4)	0.0554(2)	0.0226(1)
256	3.8	1.6	-1.122(2)	0.3431(5)	0.1244(4)	0.0470(2)	0.01837(9)
256	3.85	1.6	-1.040(2)	0.3225(5)	0.1110(3)	0.0401(2)	0.01501(8)
256	3.9	1.6	-0.968(2)	0.3037(7)	0.0993(3)	0.0343(2)	0.01236(7)
500	3.75	1.26	-1.136(2)	0.3268(6)	0.1116(3)	0.0394(2)	0.01431(8)
500	3.8	1.26	-1.041(2)	0.3003(6)	0.0954(4)	0.0316(2)	0.01084(7)
500	3.85	1.26	-0.953(2)	0.2752(7)	0.0811(3)	0.0252(1)	0.00812(6)
500	3.9	1.26	-0.873(2)	0.2505(6)	0.0683(3)	0.0198(1)	0.00600(5)
729	3.75	1	-1.107(2)	0.3088(6)	0.0993(4)	0.0329(2)	0.01122(7)
729	3.8	1	-1.009(2)	0.2798(7)	0.0827(4)	0.0254(2)	0.00810(6)
729	3.85	1	-0.916(2)	0.2499(7)	0.0672(4)	0.0191(1)	0.00564(5)
1372	3.8	1	-0.961(2)	0.2445(7)	0.0633(3)	0.0171(1)	0.00479(5)
1372	3.83	1	-0.905(2)	0.2240(6)	0.0538(3)	0.0136(1)	0.00358(3)
1372	3.86	1	-0.855(2)	0.2050(7)	0.0457(3)	0.0109(1)	0.00270(3)

intermediate discretization procedure. We checked that they are within the error bars equal to the averages obtained by the weighting procedure (4).

Error bars on the direct averages are obtained by averaging the subaverages over larger blocks and calculating the standard deviation from the block averages. The block size is increased until the standard deviation becomes independent of the block size. A block size of 32 (i.e., blocks of 3200 consecutive energy measurements and 1600 consecutive measurements of the magnetization moments) proved sufficiently large to obtain independent averages of u and the m^k.

For an error analysis of the results obtained from histogram reweighting, we averaged P over and stored it after blocks of 2×10^4 sweeps. The microcanonical magnetization moments were averaged over and stored after blocks of 10^4 consecutive Wolff updates. A typical run thus yields 50 measurements of the energy distribution and the microcanonical magnetization moments. Combining simulations at different temperatures we can reweight the block averages of the P and use (4) with the corresponding microcanonical block averages of the m^k to obtain about 50 estimates of, e.g., $\langle u \rangle$ and $\langle m^k \rangle$. These serve to calculate error bars.

In particular, we can in this way calculate error bars on the canonical averages $\langle u \rangle$ and $\langle m^k \rangle$ for the N, n, and T at which we performed the simulation. These error bars are typically within 10% of the error bars obtained from the direct averages. This indicates that the block averages of P and $\langle m^k \rangle_{mc}$ are quasi-independent.

To calculate the susceptibility χ,

$$\chi = \frac{L^3}{k_B T}(\langle m^2 \rangle - \langle m \rangle^2) \tag{5}$$

(L is the linear length of the system, k_B is Boltzmann's constant) or the Binder parameter u_4,

$$u_4 = 1 - \frac{\langle m^4 \rangle}{3\langle m^2 \rangle^2}, \tag{6}$$

we first calculate the average moments $\langle m^k \rangle$ from all the data and then calculate χ or u_4 from (5) and (6), respectively. Alternatively, one could use block averages of the m^k to calculate block averages for χ and u_4 and subsequently average over the blocks. However, the expectation value for a block average of χ and u_4 depends on the size of the blocks (this holds in principle for all nonlinear combinations of the $\langle m^k \rangle$). This effect is observable and leads, e.g., to a systematically decreasing estimate of u_4 with increasing block size. One has to extrapolate to infinite block size to account for this systematic bias. We checked that within error bars this extrapolation is identical to the use of (5) and (6) with the $\langle m^k \rangle$ obtained from averages over entire runs. To obtain error bars on χ and u_4 we did use the block averages of these quantities to calculate standard deviations.

The random number generator (RNG) we used is the subtract with carry (SWC) generator [18,19]. Since this RNG was found to perform poorly in a simulation of the two-dimensional (2D) Ising model with the Wolff algorithm [19] we tested it against a RNG which is believed to be superior [20,21]. The latter is based on two binary feedback shift registers, one of length 9689, the other of length 127, which are combined by means of the exclusive-or operation [20]. We repeated two runs with this RNG. As starting configurations we used the last configuration of the corresponding run with the SWC RNG. The results are listed in Table IV, which shows good agreement between the RNG's.

Simulations of systems smaller than 1372 particles ran on a Cray YMP-EL. Most of the $N = 1372$ systems and all of the $N = 2916$ systems ran on a Cray C-98.

III. RESULTS FOR THE DENSITY $n = 0.6$

We first give the results for the density $n = 0.6$ for which we have the largest range of system sizes. The parameters of the simulations we carried out at this density are listed in Table II together with results for the average energy per particle and the average magnetization moments.

Figure 1 shows the Binder parameter u_4 as a function of T for the five system sizes. The intersection points of the curves give an estimate of the critical temperature T_c [22]. The curves (and hence the intersection points) are obtained by applying the multihistogram reweighting technique to the energy distributions P that are averaged over an entire run. Error bars on the intersection points are obtained by reweighting the block averages of P and using the corresponding block averages $\langle m^k \rangle_{mc}$. This gives, e.g., for $N = 108$, 60 curves of u_4 versus T. For $N = 256$ it gives 50 such curves since 50 is the minimum number of block averages at each temperature (see Table II). Intersecting the nth curve for $N = 108$ with the nth curve for $N = 256$ we obtain 50 intersection points. From

TABLE IV. Comparison of two random number generators (RNG's). SWC denotes the subtract with carry RNG; CSR denotes the RNG with combined shift registers; n denotes the density of the system. The density of the first two systems is $n = 256/(7.15^3)$ which is slightly larger than 0.7. The meaning of the other columns is identical to the corresponding columns in Tables I–III. The third row is also listed in Table II.

RNG	n	N	T	N_S 10^6	$\langle u \rangle$	$\langle m \rangle$	$\langle m^2 \rangle$	$\langle m^3 \rangle$	$\langle m^4 \rangle$
SWC	0.7004	256	3.8	1.12	-1.127(2)	0.3440(6)	0.1251(4)	0.0474(2)	0.0186(1)
CSR	0.7004	256	3.8	0.8	-1.126(3)	0.3439(8)	0.1250(5)	0.0473(3)	0.0185(1)
SWC	0.6	1372	3.16	1.12	-0.898(2)	0.2487(6)	0.0654(3)	0.0179(1)	0.00508(4)
CSR	0.6	1372	3.16	0.96	-0.898(2)	0.2486(7)	0.0654(3)	0.0179(1)	0.00509(4)

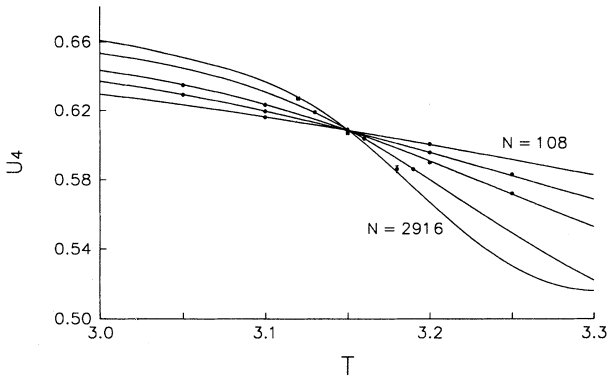

FIG. 1. The Binder parameter u_4 versus the temperature T for the five system sizes at the density $n = 0.6$. The dots are averages over individual simulations, the curves result from histogram reweighting. Error bars on the dots are omitted when smaller than the symbol size. The curves become flatter for smaller system sizes.

these we calculate the error bar on the intersection point between the $N = 108$ and $N = 256$ curves in Fig. 1. The procedure for the other intersection points is identical.

FSS predicts that the intersection point $T_i(b)$ between the curve for a system of N particles and the curve for N' particles [with $b = (N'/N)^{1/3}$, $N' > N$] equals T_c plus a correction: $T_i(b) = T_c + c/\ln b$ with c a constant [12,13,22]. A linear least squares fit [23] of the intersection points with $N = 108$ to this relation yields $T_c = 3.153(3)$, $c = (-1 \pm 2) \times 10^{-3}$, with a goodness of fit $Q = 0.84$ [12,13]. Error bars on fitted parameters are the square roots of the variances of those parameters. The variances are returned by the fit routine [23]. The same fit to the intersection points with $N = 256$ yields $T_c = 3.151(3)$, $c = (5 \pm 19) \times 10^{-4}$, with $Q = 0.69$. A fit of the value of the Binder parameter at

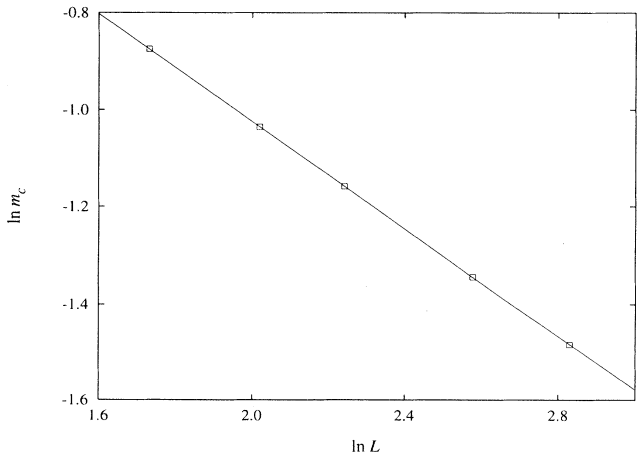

FIG. 2. ln-ln plot of the magnetization at T_c, m_c, versus the linear system size L. The squares are results for the five system sizes at the density $n = 0.6$ and the estimate $T_c = 3.145$. Error bars are smaller than the symbol size. The line is the straight line fit to the points.

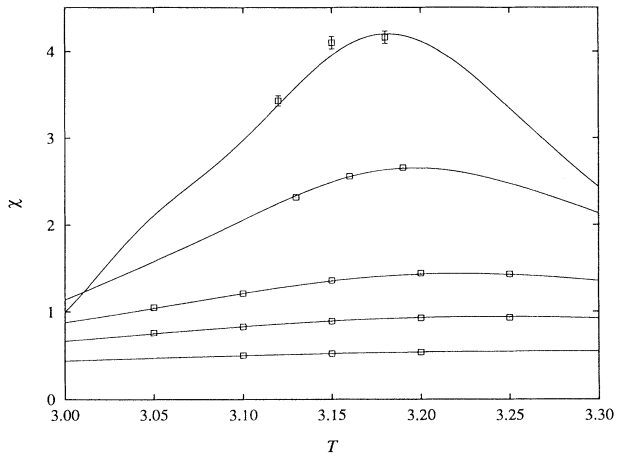

FIG. 3. The susceptibility χ versus the temperature T for the five system sizes at the density $n = 0.6$. The squares are averages over individual simulations, the curves result from histogram reweighting. Error bars on the squares are omitted when smaller than the symbol size. The susceptibility increases with increasing system size. Histogram reweighting for the largest systems down to $T = 3$ is evidently unreliable, e.g., the crossing of the curves for $N = 1372$ and $N = 2916$ is an artifact of reweighting too far away from the temperatures at which the simulations were carried out.

the intersection point u_{4i} to $u_{4i}(b) = u_{4c} + c/\ln b$ yields $u_{4c} = 0.6081(8)$, $c = (2 \pm 5) \times 10^{-4}$, $Q = 0.96$ for intersections with the $N = 108$ curve. The $N = 256$ curve yields $u_{4c} = 0.608(1)$, $c = (-1 \pm 6) \times 10^{-4}$, $Q = 0.80$.

FSS predicts the magnetization at T_c, m_c, to vary with the linear system size L as $m_c \propto L^{-\beta/\nu}$ with β and ν the magnetization and correlation length exponents, respectively [22]. A straight line fit of $\ln m_c$ versus $\ln L$ is best ($Q = 0.88$) for an estimate of $T_c = 3.145$ and gives $\beta/\nu = 0.5546(17)$. For an estimate $T_c = 3.14$ we find $\beta/\nu = 0.5402(16)$, $Q = 0.14$, while the estimate

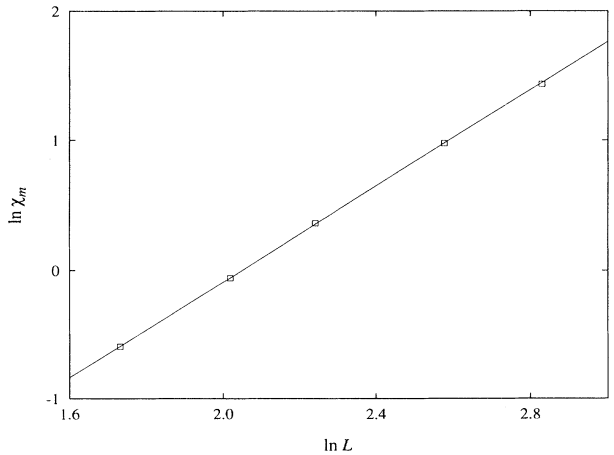

FIG. 4. ln-ln plot of the maxima of the susceptibility χ_m versus the linear system size L. The squares denote the maxima of the five curves in Fig. 3. Error bars are smaller than the symbol size. The line is the straight line fit to the squares.

$T_c = 3.15$ yields $\beta/\nu = 0.5690(17)$ with $Q = 0.32$; see Fig. 2. Straight line fits of the higher moments $\langle m^k \rangle$ at T_c ($k = 2, 3, 4$) all yield best fits for $T_c = 3.145$ and identical values for β/ν.

The susceptibility χ (5) has, as a function of T, a maximum χ_m; see Fig. 3. According to FSS $\chi_m \propto L^{\gamma/\nu}$ with $\gamma/\nu = 3 - 2(\beta/\nu)$ and γ the susceptibility exponent [22]. A straight line fit of $\ln \chi_m$ versus $\ln L$ yields $\gamma/\nu = 1.856(9)$ with $Q = 0.38$; see Fig. 4. The ratio γ/ν can also be estimated from $\chi_c = \chi(T_c)$ for which the same scaling as for χ_m is predicted. Straight line fits of $\ln \chi_c$ versus $\ln L$ are good fits (with $Q > 0.6$) for a wide range of temperatures although with a systematic variation in the resulting γ/ν. If we take T_c in the range $3.145 < T_c < 3.155$ we estimate $\gamma/\nu = 1.84(2)$. The ratio χ_c/χ_m is according to FSS independent of L for L sufficiently large [22]. Fitting this ratio for the five system sizes to a constant c we obtain a best fit $c = 0.953(1)$ ($Q = 0.38$) for the estimate $T_c = 3.155$. For the estimate $T_c = 3.15$ the fit worsens to $Q = 0.03$ [$c = 0.946(1)$] while for $T_c = 3.16$ we have $Q = 0.11$ [$c = 0.958(1)$].

The ratio $1/\nu$ can, e.g., be obtained from the minima in $\partial\langle m \rangle/\partial T$ as a function of T. The derivative was calculated from the energy-magnetization correlation [24]:

$$\frac{\partial\langle m \rangle}{\partial T} = \frac{N}{k_B T^2}(\langle mu \rangle - \langle m \rangle \langle u \rangle). \tag{7}$$

We checked that this way of obtaining $\partial\langle m \rangle/\partial T$ gives the same results as taking finite differences $\Delta m/\Delta T$ for ΔT small enough.

The minima are predicted to scale as $(\partial\langle m \rangle/\partial T)_{\min} \propto L^{(1-\beta)/\nu}$. However, the curve of $\ln(\partial\langle m \rangle/\partial T)_{\min}$ versus $\ln L$ shows a pronounced curvature leading to the poor value $Q = 0.01$ for a straight line fit. Limiting the fit to the $N = 500$, 1372, and 2916 systems yields $Q = 0.58$ and $(1 - \beta)/\nu = 0.86(3)$; see Fig. 5. With $\beta/\nu = 0.56(2)$ we obtain $1/\nu = 1.42(3)$. The magnetization derivative $\partial\langle m \rangle/\partial T$ at T_c should scale in the same fashion but yields once more curved lines on a ln-ln plot for all reasonable estimates of T_c. Even if we limit the fit to the three largest systems we retain rather poor fits: $Q = 0.21$–0.24 with $(1 - \beta)/\nu = 0.86(2)$ for all estimates of T_c in between 3.13 and 3.16. If we inspect the slope $\partial u_4/\partial T$ at T_c, which FSS predicts to scale as $(\partial u_4/\partial T)_{T_c} \propto L^{1/\nu}$, we find good straight line fits of $\ln(\partial u_4/\partial T)_{T_c}$ versus $\ln L$ for a large range of choices for T_c. If we take $T_c = 3.15$ we estimate $1/\nu = 1.40(3)$.

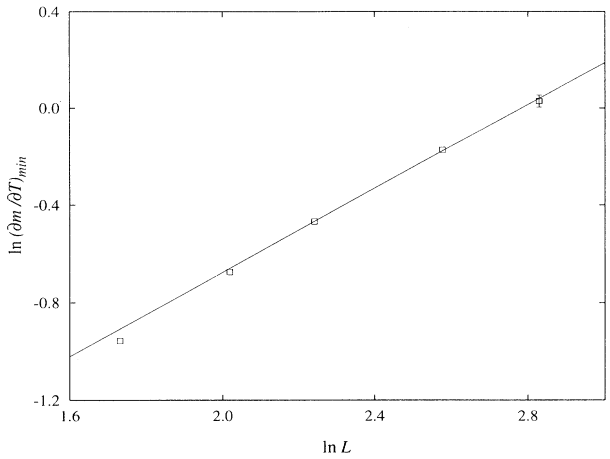

FIG. 5. ln-ln plot of the minima of $\partial\langle m \rangle/\partial T$ versus the linear system size L. The squares are for the five systems at the density $n = 0.6$. Error bars are omitted when smaller than the symbol size. The line is the straight line fit to the data for the largest three system sizes.

Our final estimates are $T_c = 3.150(5)$, $u_{4c} = 0.6081(8)$, $\beta/\nu = 0.56(2)$, $\gamma/\nu = 1.85(1)$, and $1/\nu = 1.41(3)$ for the density $n = 0.6$. They are summarized in Table V which also gives the values for the lattice Heisenberg model. They turn out to be slightly different. The data-collapse plots in Fig. 6 and Fig. 7 emphasize that the simulations favor for the Heisenberg fluid our estimate of γ/ν above the value for the lattice model.

We tried whether our data are compatible with the lattice Heisenberg exponents and the inclusion of corrections to FSS. We fitted χ_m to $\chi_m(L) = c_1 L^{\gamma/\nu} + c_2 L^{-y+(\gamma/\nu)}$ with γ/ν fixed at the lattice Heisenberg value 1.975 [12–14]. If we fix y at values $0 < y \leq 0.1$ the fit routine gives reasonable fits ($Q = 0.51$ for $y = 0.01$ decreasing to $Q = 0.43$ for $y = 0.1$) but it gives $c_1 < 0$ which is unphysical. For $y = 0.2$ we obtain $c_1 = 0.0066(9)$, $c_2 = 0.016(1)$, $Q = 0.35$. The goodness of fit decreases further with increasing y with, e.g., $Q = 0.21$ for $y = 0.4$. Hence the assumption of lattice Heisenberg critical behavior with corrections to scaling does not fit the data better. We recall that if we fit $\chi_m(L)$ to $\chi_m(L) = c_1 L^{\gamma/\nu}$ with c_1 and γ/ν free parameters we obtain $c_1 = 0.0222(4)$, $\gamma/\nu = 1.856(9)$, $Q = 0.38$.

TABLE V. Summary of results. n is the density; T_c the critical temperature; u_{4c} the critical value of the Binder parameter; β/ν, γ/ν, and $1/\nu$ are exponent ratios. The last row gives the results for the lattice Heisenberg model from Refs. [12–14]. The critical temperature in this row is for the simple cubic lattice [$T_c = 2.0542(2)$ for the bcc lattice [14]].

n	T_c	u_{4c}	β/ν	γ/ν	$1/\nu$
0.4	1.940(5)	0.6130(8)	0.55(2)	1.86(3)	1.35(5)
0.6	3.150(5)	0.6081(8)	0.56(2)	1.85(1)	1.41(3)
0.7	3.79(1)	0.605(2)	0.55(2)	1.84(3)	1.42(3)
lattice	1.44293(8)	0.6217(8)	0.514(1)	1.973(2)	1.421(5)

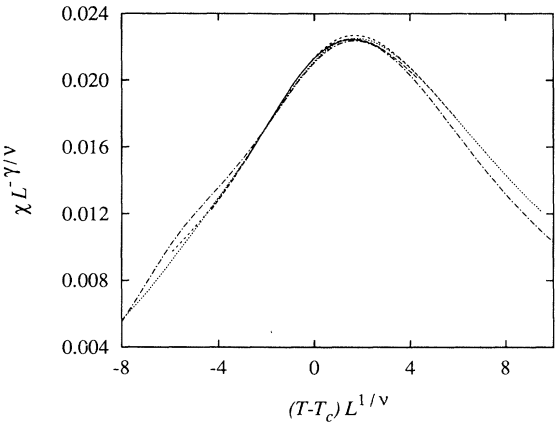

FIG. 6. Data collapse plot for the susceptibilities of Fig. 3. The collapse was carried out with our estimates $T_c = 3.15$, $\gamma/\nu = 1.85$, and $1/\nu = 1.41$.

IV. RESULTS FOR THE DENSITIES $n = 0.4$ AND $n = 0.7$

The analysis for $n = 0.4$ and $n = 0.7$ is similar although somewhat less convincing because of the absence of an $N = 2916$ system. We first discuss the case $n = 0.4$.

A. $n = 0.4$

The fit of the intersection points of the Binder parameter yields $T_c = 1.940(2)$, $c = (9 \pm 13) \times 10^{-4}$, $Q = 0.51$ for the critical temperature and $u_{4c} = 0.6130(8)$, $c = (-2 \pm 4) \times 10^{-4}$, $Q = 0.62$ for the critical Binder parameter. These data are for the intersection with the $N = 108$ curve. We only have two systems larger than the $N = 256$ system and therefore we have too few intersection points (namely, two) to carry out a fit. Nevertheless,

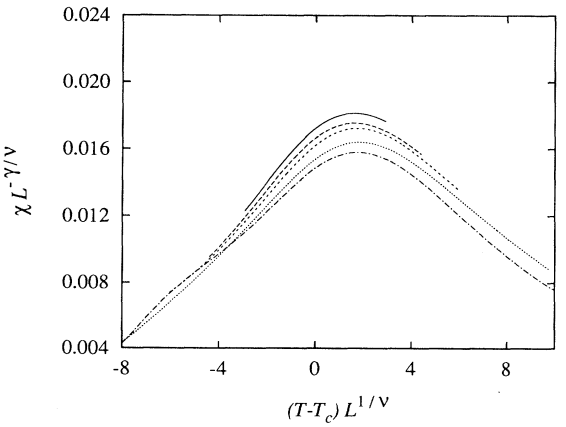

FIG. 7. As Fig. 6 but with the collapse carried out with $T_c = 3.15$ and the lattice Heisenberg exponents $\gamma/\nu = 1.973$ and $1/\nu = 1.421$. The curves are shifted downwards with increasing system size: the top curve is for the $N = 108$ system, the bottom curve for $N = 2916$.

the two intersection points [$T_i = 1.953(3)$, $u_{4i} = 0.612(1)$ for $N = 500$ and $T_i = 1.940(1)$, $u_{4i} = 0.6130(5)$ for $N = 1372$] are in good agreement with the estimates of T_c and u_{4c}.

Straight line fits of $\ln m_c$ versus $\ln L$ yield best results for the estimate of $T_c = 1.94$: $Q = 0.58$ with $\beta/\nu = 0.5567(18)$. Putting $T_c = 1.945$ gives $\beta/\nu = 0.5741(19)$, $Q = 0.02$; $T_c = 1.935$ gives $\beta/\nu = 0.5396(18)$, $Q = 0.42$; while $T_c = 1.93$ gives $\beta/\nu = 0.5230(18)$, $Q = 0.01$. Straight line fits of the higher moments $\ln\langle m^k\rangle$ versus $\ln L$ give identical results.

The maxima χ_m of the susceptibility yield $\gamma/\nu = 1.880(8)$ with a goodness of the straight line fit $Q = 0.42$. The susceptibilities at T_c, χ_c, give reasonable to excellent straight line fits for a broad range of estimates of T_c. If we estimate T_c in the range $1.935 < T_c < 1.945$ we obtain $\gamma/\nu = 1.86(3)$. The fit of the susceptibility ratio χ_c/χ_m to a system-size independent constant c gives a good fit for $T_c = 1.945$ [$Q = 0.65$, $c = 0.937(1)$] and dramatically worse fits for $T_c = 1.94$ [$Q = 0.02$, $c = 0.928(1)$] and $T_c = 1.95$ [$Q = 0.01$,$c = 0.945(1)$].

A straight line fit of $\ln(\partial\langle m\rangle/\partial T)_{\min}$ versus $\ln L$ yields $(1-\beta)/\nu = 0.81(1)$ with $Q = 0.36$. As for the density $n = 0.6$ in Fig. 5, the points for this density display some curvature as well. Omitting the point for the $N = 108$ system from the fit gives $(1-\beta)/\nu = 0.82(2)$, $Q = 0.78$. If we increase the error bar to 0.03 in anticipation of a systematic bias due to the curvature and combine $(1-\beta)/\nu = 0.82(3)$ with the estimate $\beta/\nu = 0.55(2)$ we obtain $1/\nu = 1.37(4)$.

Similarly, straight line fits of $\ln \partial\langle m\rangle/\partial T$ at T_c versus $\ln L$ are poor ($Q \leq 0.05$) for all reasonable estimates of T_c due to a curvature in the data. If we limit the fit to the $N = 256$, 500, and 1372 systems we obtain $(1-\beta)/\nu = 0.812(14)$, $Q = 0.36$ for $T_c = 1.93$; $(1-\beta)/\nu = 0.827(13)$, $Q = 0.49$ for $T_c = 1.94$; $(1-\beta)/\nu = 0.828(14)$, $Q = 0.45$ for $T_c = 1.95$.

The data for $(\partial u_4/\partial T)_{T_c}$ give good fits for very low estimates of T_c (e.g., $Q = 0.63$ for $T_c = 1.93$, $Q = 0.87$ for $T_c = 1.92$) but a rather poor $Q = 0.14$ for $T_c = 1.94$. If we limit the fit to the largest three system sizes we obtain $1/\nu = 1.33(3)$ with $Q = 0.73$.

Combining these results we finally estimate $T_c = 1.940(5)$, $u_{4c} = 0.6130(8)$, $\beta/\nu = 0.55(2)$, $\gamma/\nu = 1.86(3)$, and $1/\nu = 1.35(5)$ for $n = 0.4$.

B. $n = 0.7$

The situation for $n = 0.7$ is somewhat more worrisome. In general, the various straight line fits have much lower Q values than the corresponding fits at $n = 0.4$ and $n = 0.6$ because of an increased scatter of the data points.

This is already borne out by the analysis of the intersections of the Binder parameters. The fit of the temperatures $T_i(b)$ at the intersection point yields $T_c = 3.791(3)$, $c = (3 \pm 2) \times 10^{-3}$, $Q = 0.09$ for the intersections with the $N = 108$ curve. Figure 8 shows the intersection points and the fit. It demonstrates that the situation is not dissimilar to the situation for $n = 0.4$ and $n = 0.6$, with comparable error bars on the T_i and a comparable

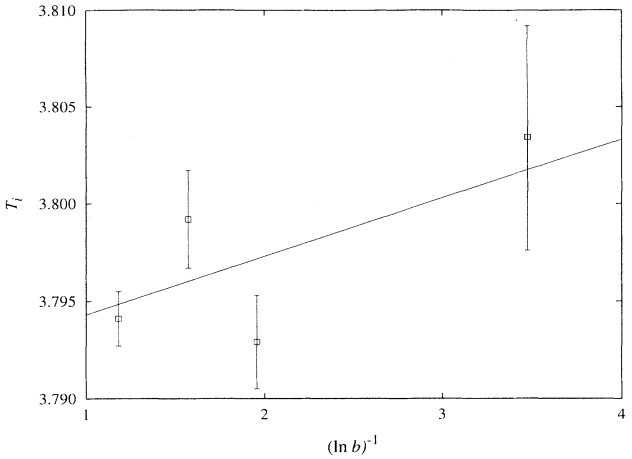

FIG. 8. Intersection point temperatures T_i versus $1/\ln b$. The intersections are between the curve for $N = 108$ and the curves for larger systems; $b = (N/108)^{1/3}$. The data are for the density $n = 0.7$. The line is the straight line fit to the four intersection points.

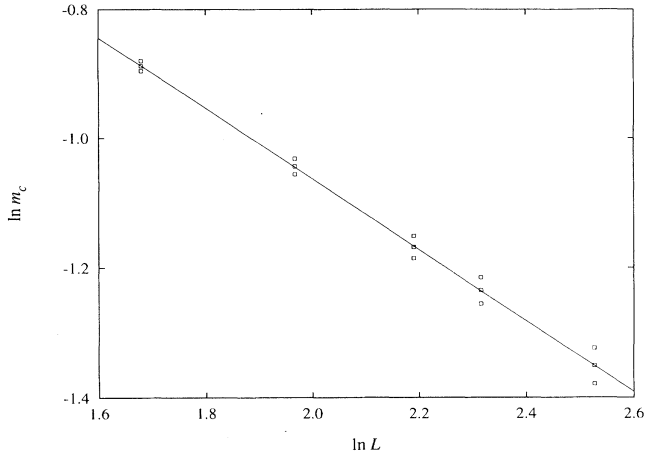

FIG. 9. ln-ln plot of the magnetization at T_c, m_c, versus the linear system size L. The squares are results for the five system sizes at the density $n = 0.7$ and three estimates of T_c: $T_c = 3.77, 3.78, 3.79$. At any L, m_c decreases for a higher estimate of T_c. Error bars on the squares do not exceed the symbol size. The line is the straight line fit to the points for $T_c = 3.78$. The points for the other estimates of T_c show an increased curvature.

slope $c = (3 \pm 2) \times 10^{-3}$. However, whereas the intersection temperatures line up at $n = 0.4$ and $n = 0.6$ to give a credible straight line fit, they fail to do so at this density. To a lesser degree, this concern holds also for the fit of the Binder parameters u_{4i} at the intersection points. The goodness of fit is $Q = 0.30$ while the fit gives $u_{4c} = 0.6056(7)$, $c = (-4 \pm 4) \times 10^{-4}$. The intersection points with the $N = 256$ curve show the same deficiency. They give $T_c = 3.797(5)$, $c = (-2 \pm 2) \times 10^{-3}$, $Q = 0.03$ for the critical temperature and $u_{4c} = 0.605(1)$, $c = (5 \pm 5) \times 10^{-4}$, $Q = 0.10$ for the critical Binder parameter.

For the critical magnetization m_c we find the best fit for $T_c = 3.78$ with $\beta/\nu = 0.547(2)$, $Q = 0.22$. Fits for $T_c = 3.77$ [$\beta/\nu = 0.527(2)$, $Q = 0.06$] and $T_c = 3.79$ [$\beta/\nu = 0.568(2)$, $Q = 0.009$] are significantly worse. Figure 9 shows that the very moderate Q value for $T_c = 3.78$ is not due to a curvature in the data points but to the scatter of the points around the fit (the scatter is almost not noticeable on the scale of Fig. 9). In contrast, the estimates $T_c = 3.77$ and $T_c = 3.79$ lead to a curvature in the data points.

The maxima of the susceptibility χ_m give rise to a fit with $\gamma/\nu = 1.843(7)$ and $Q = 0.36$. The susceptibilities at T_c, χ_c, lead to straight line fits with $Q = 0.06$–0.09 for all estimates of T_c in the range $3.78 < T_c < 3.82$. Figure 10 displays the data points and the fit for $T_c = 3.79$ [this fit has $\gamma/\nu = 1.820(7)$, $Q = 0.08$]. It can be seen that the poor Q value results from scatter of the data points around the straight line fit rather than a systematic curvature in the data.

The fit of the susceptibility ratio χ_c/χ_m to a system-size independent constant c is best for $T_c = 3.8$ [$c = 0.9634(9)$, $Q = 0.45$] with $c = 0.955(1)$, $Q = 2 \times 10^{-5}$ for $T_c = 3.79$ and $c = 0.9717(8)$, $Q = 0.06$ for $T_c = 3.81$.

We have not attempted to analyze the minima of $\partial\langle m\rangle/\partial T$ since these minima occur mainly at temperatures outside the range of temperatures at which we performed simulations. For example, for $N = 1372$ we find the minimum at $T = 3.770(5)$ whereas simulations have been performed at $T = 3.8$ and higher temperatures (see Table III). This requires that we rely strongly on extrapolation by histogram reweighting. In view of the rapid deterioration of the $\partial\langle m\rangle/\partial T$ data under extrapolation we found this an unreliable procedure.

The derivative $\partial\langle m\rangle/\partial T$ at T_c yields, as for $n = 0.4$ and $n = 0.6$, very poor straight line fits because of a curvature in the data. Limiting the fit to the $N = 500$, $N = 729$, and $N = 1372$ systems only we obtain $(1 - \beta)/\nu = 0.87(3)$, $Q = 0.10$ for $T_c = 3.79$. The values of

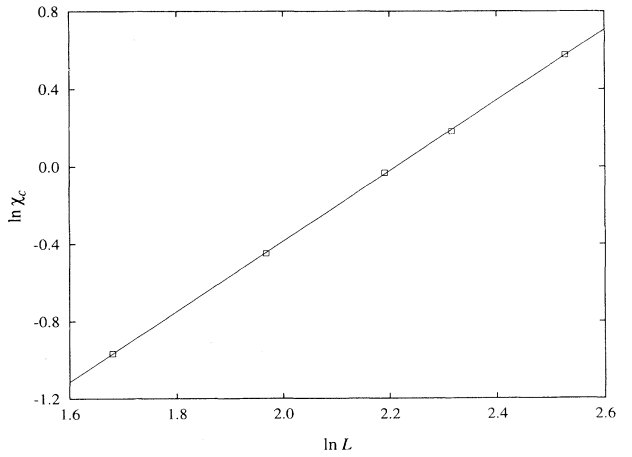

FIG. 10. ln-ln plot of the susceptibility at T_c, χ_c, versus the linear system size L. The squares are for the estimate $T_c = 3.79$ and the density $n = 0.7$. Error bars do not exceed the symbol size. The line is the straight line fit to the squares.

$(1-\beta)/\nu$ for $T_c = 3.78$ and $T_c = 3.80$ are identical within error bars with $Q = 0.08$ and $Q = 0.14$, respectively. If we combine this estimate of $(1-\beta)/\nu$ with the estimate $\beta/\nu = 0.55(2)$ we obtain $1/\nu = 1.42(3)$.

The derivative of the Binder parameter $\partial u_4/\partial T$ at T_c yields $1/\nu = 1.36(2)$, $Q = 0.35$ for $T_c = 3.78$; $1/\nu = 1.41(2)$, $Q = 0.27$ for $T_c = 3.79$; and $1/\nu = 1.44(2)$, $Q = 0.16$ for $T_c = 3.80$. It can again be checked that these rather moderate values of Q are caused by a scatter in the data rather than by a curvature.

Hence we have seen that the data possess a scatter that is not entirely justified by the error bars. One could argue conversely that the error bars are underestimated but we have no more direct evidence for this. It could also be that the scatter is a systematic effect that becomes stronger with increasing density for reasons that are not well understood.

Or final estimates for the density $n = 0.7$ are $T_c = 3.79(1)$, $u_{4c} = 0.605(2)$, $\beta/\nu = 0.55(2)$, $\gamma/\nu = 1.84(3)$, and $1/\nu = 1.42(3)$.

V. CONCLUSIONS

We have performed MC simulations of a Heisenberg fluid which appear to be the most accurate simulations of a magnetic fluid to date. Three points on the magnetic order-disorder line in the density range 0.4–0.7 are obtained. These results provide tests for theoretical predictions based, e.g., on the mean spherical approximation [3], hypernetted chain integral equation [1], mean field theory [4,5], or modifications of the latter [5,25].

A meaningful comparison with the previous MC results of Lomba *et al.* is difficult due to the use of different potential cutoffs: 4.5σ in Ref. [1] compared to 2.5σ in the present work. Figure 3 in Ref. [1] shows $T_c \approx 17$ which in our units of temperature (which differ by a factor of 3) becomes $T_c \approx 5.7$ for the density $n = 0.7$. This is significantly larger than our estimate $T_c = 3.79(1)$. The increase of T_c seems sensible since one expects that a longer interaction range makes it easier for the spins to order and hence yields a larger critical temperature. In fact, an increase of T_c with an increasing interaction range has been reported for various systems [26,27].

It is likely that the estimate of $T_c \approx 5.7$ of Lomba *et al.* is an underestimate. Namely, Table III shows that, for our system with a cutoff 2.5σ, an estimate of T_c as the temperature at which $\langle m \rangle \approx 0.5$ for a 500 particle system yields a T_c far below our estimate $T_c = 3.79(1)$.

The improved quality of our simulations makes it possible to estimate critical exponents. An *a priori* guess is that they are equal to the lattice Heisenberg exponents. Fisher renormalization arguments [9] also predict them to remain unchanged since the specific heat exponent α for the lattice Heisenberg model is negative [12–14]. However, our simulations disagree with this prediction and predict novel exponents, shown in Table V. It is possible that these "exponents" are effective exponents for the modest system sizes that we could study. In that case the asymptotic FSS scaling region would be visible only for larger systems. Nevertheless, it is encouraging that our estimates for exponent ratios are the same for all three densities. It is also encouraging that they satisfy the exponent relation $(2\beta + \gamma)/\nu = d$ with the dimension $d = 3$. Besides exponents, our values for the critical Binder parameter are markedly smaller than the value for the lattice Heisenberg model. It is puzzling that, whereas our estimates for $n = 0.6$ and $n = 0.7$ agree, the value for $n = 0.4$ is in between those and the value for the lattice Heisenberg model.

Absent from our study is an analysis of $\langle u \rangle$, the specific heat c_V, or higher moments of the energy distribution P to determine α. Hyperscaling gives $\alpha/\nu = (2/\nu) - d = -0.18(6)$ using the estimate $1/\nu = 1.41(3)$ for $n = 0.6$. This small and negative value implies that the analytic background in, e.g., $\langle u \rangle$ and c_V will be important and that therefore nonlinear three-parameter fits should be used to extract α [12,13]. These fits are even difficult in simulations of the lattice Heisenberg model [12,13] and are not feasible in our case where at best we have five different system sizes. We rather rely on the hyperscaling result.

Besides a study of larger systems, other extensions of this work could contribute to a better understanding of the transition studied here. Our simulations focused entirely on the magnetization as the order parameter that describes the transition. Alternatively, one might question whether in, e.g., a grand canonical ensemble the density has a singular behavior at the transition and can serve as an order parameter as well. Such an investigation would also be a suitable means to locate the first-order liquid-vapor line. Ultimately, one would like to assess the interplay between density and magnetization that was the subject of Refs. [1,5]. We aim to study the density as order parameter in our next simulation.

ACKNOWLEDGMENTS

We thank D. Levesque, H. J. Hilhorst, H. W. J. Blöte, J. R. Heringa, and G. Stell for their interest and their suggestions. The random number generator with combined shift registers was kindly supplied by H. W. J. Blöte. Computing time on the C-98 was granted by the Institut de Développement et des Ressources en Informatique Scientifique (IDRIS). M.J.P.N. benefited from a grant of the French government. The Laboratoire de Physique Théorique et Hautes Energies is associé au Centre National de la Recherche Scientifique (CNRS) (URA 0063).

[1] E. Lomba, J.J. Weis, N.G. Almarza, F. Bresme, and G. Stell, Phys. Rev. E **49**, 5169 (1994).
[2] E. Lomba, J.J. Weis, and G. Stell, Phys. Rev. E **50**, 3853 (1994).
[3] J.S. Høye and G. Stell, Phys. Rev. Lett. **36**, 1569 (1976).
[4] P.C. Hemmer and D. Imbro, Phys. Rev. A **16**, 380 (1977).
[5] J.M. Tavares, M.M. Telo da Gama, P.I.C. Teixeira, J.J. Weis, and M.J.P. Nijmeijer, Phys. Rev. E **52**, 1915 (1995); **52**, 5716(E) (1995).
[6] R.B. Stinchcombe, in *Phase Transitions and Critical Phenomena*, edited by C. Domb and J.L. Lebowitz (Academic Press, London, 1983), Vol. 7.
[7] G. Jug, Phys. Rev. B **27**, 609 (1983).
[8] A. Shpot, Phys. Lett. A **133**, 125 (1988); **142**, 474 (1989).
[9] M.E. Fisher, Phys. Rev. **176**, 257 (1968).
[10] T.W. Burkhardt and H.J.F. Knops, Phys. Rev. B **15**, 1602 (1977).
[11] M. Kaufman, R.B. Griffiths, J.M. Yeomans, and M.E. Fisher, Phys. Rev. B **23**, 3448 (1981).
[12] P. Peczak, A.M. Ferrenberg, and D.P. Landau, Phys. Rev. B **43**, 6087 (1991).
[13] C. Holm and W. Janke, Phys. Rev. B **48**, 936 (1993).
[14] K. Chen, A.M. Ferrenberg, and D.P. Landau, Phys. Rev. B **48**, 3249 (1993).
[15] M.J.P. Nijmeijer and J.J. Weis, Phys. Rev. Lett. **75**, 2887 (1995).
[16] U. Wolff, Phys. Rev. Lett. **62**, 361 (1989).
[17] A.M. Ferrenberg and R.H. Swendsen, Phys. Rev. Lett. **63**, 1195 (1989).
[18] G. Marsaglia, B. Narasimhan, and A. Zaman, Comput. Phys. Commun. **60**, 345 (1990).
[19] A.M. Ferrenberg, D.P. Landau, and Y.J. Wong, Phys. Rev. Lett. **69**, 3382 (1992).
[20] H.W.J. Blöte and J.R. Heringa (private communication).
[21] J.R. Heringa, H.W.J. Blöte, and A. Compagner, Int. J. Mod. Phys. C **3**, 561 (1992).
[22] K. Binder, Z. Phys. B **43**, 119 (1981).
[23] W.H. Press, B.P. Flannery, S.A. Teukolsky, and W.T. Vetterling, *Numerical Recipes—The Art of Scientific Computing* (Cambridge University Press, Cambridge, England, 1986).
[24] A.M. Ferrenberg and D.P. Landau, Phys. Rev. B **44**, 5081 (1991).
[25] L. Feijoo, C.W. Woo, and V.T. Rajan, Phys. Rev. B **22**, 2404 (1980).
[26] M.H.J. Hagen and D. Frenkel, J. Chem. Phys. **101**, 4093 (1994).
[27] E. Lomba and N.G. Almarza, J. Chem. Phys. **100**, 8367 (1994).